# Towards Non-Linear Unsteady Vortex Lattice Method (NL-UVLM) for rotary-wing aerodynamics

Vincent Proulx-Cabana* and Eric Laurendeau†
*Polytechnique Montréal, Montréal, Québec, H3C 3A7, Canada*

**The Unsteady Vortex Lattice Method (UVLM) is a 3D Potential Method. Viscous coupling can be added to that classical method resulting in a Non-Linear Unsteady Vortex Lattice Method (NL-UVLM) to benefit from higher fidelity 2D computations instead of using sectional linear lift curve from thin airfoil theory. Viscous coupling is thus capable of modeling any aerodynamic effect that can be summarized into lift and drag 2D databases (e.g. sweep cross-flow (2.5D), compressibility, centrifugal-Coriolis effects, icing, aileron deflection). This article presents preliminary results generated with NL-UVLM compared with 3D Unsteady Reynolds Averaged Navier-Stokes (URANS 3D) on a simplified S-76 test case. Coefficient of thrust shows expected behavior compared with the UVLM classical method and the figure of merit seems to have a good agreement with URANS 3D results.**

## I. Nomenclature

| | | |
|---|---|---|
| $C_T$ | = | Coefficient of Thrust: $T/\rho_{\text{inf}}\pi R^2 V_{tip}^2$ |
| $C_Q$ | = | Coefficient of Torque: $Q/\rho_{\text{inf}}\pi R^3 V_{tip}^2$ |
| $FM$ | = | Figure of Merit: $C_{Q,ideal}/C_Q = \sqrt{\frac{C_T^3}{2}}/C_Q$ |
| $\theta_{75}$ | = | Collective angle at 75% blade span |
| $\frac{\Delta C_t}{\Delta r}$ | = | Sectional thrust coefficient |
| $C_l$ | = | Local lift coefficient: $L/\frac{1}{2}\rho_{\text{inf}} V_{local}^2 S$ |
| $C_d$ | = | Local drag coefficient: $D/\frac{1}{2}\rho_{\text{inf}} V_{local}^2 S$ |

## II. Introduction

Helicopters and smaller lifting rotor(s) unmanned aerial vehicles (UAVs) remain unequaled for missions in confined environment such as close to cliffs, buildings or aircraft carriers because of their vertical takeoff and hovering capacities. The performances of such rotary-wing aircrafts depend largely on the accuracy, flexibility and speed of the initial design tools used in phases where many configurations can be analyzed. As of today, such optimization of the aerodynamics of these rotors' blades is dragged by the unavailability of satisfactory tools. Design is usually based on low fidelity models (Blade Element Momentum Theory) that fail to capture important features of the rotor aerodynamics such as the unsteadiness, the viscous effects, the wake development and the proximity to arbitrary obstacles. There also exists high fidelity models (CFD) but their compute and mesh generation time are too prohibitive to be affordable at early design stages. These assessments have pushed researchers to turn their attention toward so called medium fidelity methods in the context of rotary-wing: Potential Methods (Source, Doublet and Vortex). In the meantime, these potential methods have recently regained attention for fixed wing applications with the alleviation of some of the classical method's limitations by including new low computational cost non-linear coupling algorithms utilizing bidimensional higher fidelity aerodynamics computations. In this work, we present initial results toward the adaptation of a C++ Non-Linear Unsteady Vortex Lattice Method (NL-UVLM) software validated for fixed wing aerodynamics to rotary-wings aerodynamics. The addition of the non-linear coupling can enable the consideration of any bidimensional aerodynamic effect on the blade, such as profile viscosity, compressibility [1], sweep cross-flow (2.5D) [2], centrifugal-Coriolis forces [3], ice accretion [4] or control surface deflection [5] in a fast aerodynamics software. Better consideration of these complex phenomenon earlier in the design process could help improve new aircraft's

*Ph.D. Candidate, Department of Mechanical Engineering, C.P. 6079, Centre-Ville, Montréal(QC), H3C 3A7, Canada
†Professor, Department of Mechanical Engineering, C.P. 6079, Centre-Ville, Montréal(QC), H3C 3A7, Canada

performances, translating in longer range, heavier payloads or longer endurance. This paper reviews the classical UVLM in the context of rotorcraft application, describes the viscous coupling algorithm, shows the methodology and finally presents preliminary results compared with 3D Unsteady Reynolds Averaged Navier-Stokes (URANS 3D) results on a simplified S-76 test case.

## III. Unsteady Vortex Lattice Method (UVLM) for rotary-wing

### A. Potential Methods

Potential methods assume inviscid and incompressible flows. Assuming a velocity potential, the governing equation is Laplace equation (1).

$$\nabla^2 \Phi = 0 \tag{1}$$

These methods enforce that flow is tangent on the surface, perturbations vanish at infinity and flow leaves the geometry smoothly (Kutta condition). Potential flow problems can be solved by placing singular elementary solutions (sources, doublets or vortex) on the boundary and determining their strength distribution.

### B. Vortex Lattice Method (VLM)

VLM is a surface generalization of Prandtl lifting line [6]. The lifting geometry and the wake are modeled with vortex panels, with the wake panels' circulation set to be the same as their corresponding geometry trailing edge panel, thus enforcing Kutta condition. In theory, wake panels extend to infinity behind the geometry. The flow tangency is computed on control points, located at the center of the three-quarter chord line on every geometry panel. The algorithm for solving VLM is:

1) Mesh lifting geometry camber line with panels. Mesh wake panels extending from trailing edge panels to very far downstream.
2) Compute velocity induced by geometry and wake panels' edges on geometry control points with Biot-Savart equation (2):

$$\vec{u}_{i,\vec{P}} = \frac{\Gamma}{4\pi} \frac{\vec{r}_1 \times \vec{r}_2}{||\vec{r}_1 \times \vec{r}_2||^2} \vec{r}_0 \cdot \left( \frac{\vec{r}_1}{||\vec{r}_1||} - \frac{\vec{r}_2}{||\vec{r}_2||} \right) \tag{2}$$

   where $\Gamma$ is the panel's vortex strength, $\vec{r}_0$ the vortex filament vector (panel's edge vector) and $\vec{r}_1$, $\vec{r}_2$ the vectors from the filament's extremities to the evaluation point.
3) Factoring $\Gamma$ from equation (2), VLM linear system of equation (3) can be constructed.

$$A\Gamma = \vec{V} \cdot \vec{n} \tag{3}$$

   Where $A$ is the influence coefficient matrix and the right hand side is the flow tangency boundary condition with $\vec{V}$ the sum of the induced and free stream velocities and $\vec{n}$ the geometry normal unit vector at the control point.
4) Solving (3) for $\Gamma$, the vortex panels' circulation strength is obtained.
5) Aerodynamic force at every panel edge can be computed using Kutta-Joukowski theorem (4).

$$\Delta F_a = \rho_\infty \Gamma \vec{V} \times \vec{r}_0 \tag{4}$$

   with $\rho_\infty$ the fluid density in the free stream and the other terms as defined above.

### C. Prandtl-Glauert compressibility correction

Potential flows assume incompressible flow, which is arguably valid up to Mach numbers of about 0.3. Above that value, compressibility effects should not be ignored. Helicopter blade tips typically operate at Mach numbers higher than 0.3. VLM implementation of Prandtl-Glauert correction to include compressibility effects given in [7] is :

1) Solve Incompressible VLM.
2) When computing the forces with Kutta-Joukowski theorem (4), correct the circulation of the panels with Prandtl-Glauert compressibility factor:

$$\Gamma_c = \frac{\Gamma_i}{\beta} \tag{5}$$

   where $\beta = \sqrt{1 - M^2}$.

### D. Unsteady Vortex Lattice Method (UVLM)

UVLM is basically a succession of VLM solutions with time stepping. During this time step, the geometry is displaced according to it's kinematic velocity, shedding new wake panels behind trailing edge panels. Then, wake panels are displaced along their local velocity. Finally, an added unsteady component of aerodynamic force can be computed at every geometry panel using unsteady Bernoulli (6):

$$\Delta F_{a,unsteady} = \rho_\infty \frac{\delta \Gamma}{\delta t} A \vec{n} \tag{6}$$

with $\frac{\delta \Gamma}{\delta t}$ the rate of change of the panel's circulation with respect to time, $A$ and $\vec{n}$ respectively the area and the normal unit vector of the panel. During wake displacement, rotor simulations are more likely to experience the singularity in the Biot-Savart equation (2) than fixed wing simulations because wake panels tend to roll up and cluster near the tip vortex beneath the rotor.

### E. Singularity smoothing

Vatistas smoothing kernel (7) can be used to remove the Biot-Savart singularity [8] by adding a smoothing radius $r_c$. In UVLM rotor simulations, small $r_c$ should be used to relieve the singularity without affecting too much the overall results. A typical value for this parameter would be between 5-10% of blade tip chord, that is, about the thickness of the profile where the tip vortexes are formed [9].

$$\vec{u}_{i,\vec{P}} = \frac{\Gamma}{4\pi} \frac{\vec{r}_1 \times \vec{r}_2}{\left(||\vec{r}_1 \times \vec{r}_2||^{2n} + ||r_c \vec{r}_0||^{2n}\right)^{\frac{1}{n}}} \vec{r}_0 \cdot \left( \frac{\vec{r}_1}{||\vec{r}_1||} - \frac{\vec{r}_2}{||\vec{r}_2||} \right) \tag{7}$$

Figure 1 shows the difference between the application of Biot-Savart Singular equation (2) and Vatistas smoothing kernel (7) on the wake displacement of a hovering rotor. The singularity induces very large displacements to some vortex filaments, some of which extend through the rotor plane, causing large unsteady aerodynamic forces. The smoothed kernel is free of these effects.

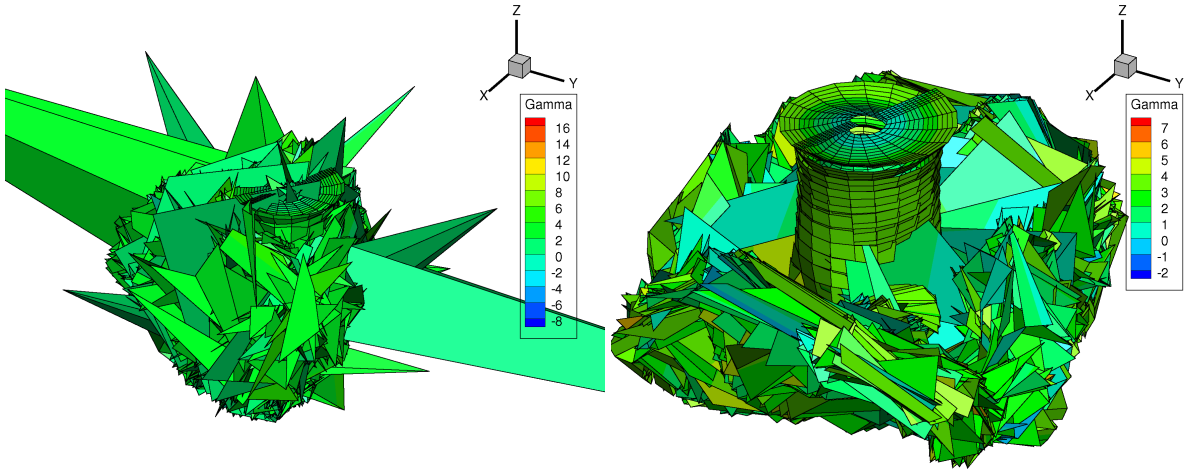


**Fig. 1 UVLM rotor simulation using a) Singular Biot-Savart b) Vatistas smoothing kernel**

## IV. Non-Linear Unsteady Vortex Lattice Method (NL-UVLM)

NL-UVLM or Viscous coupling takes advantage of higher fidelity 2D aerodynamic computations at different spanwise sections to correct the 3D method. There are two well known iterative algorithms that can achieve this task: the $\Gamma$ [10] and the $\alpha$ [11] methods.

In the $\Gamma$ method, the effective angle of attack is obtained by first computing the induced angle of attack. Section lift is interpolated at the effective angle of attack in the database. Section lift is used to update UVLM panels' circulation

directly solving for Γ in Kutta-Joukowski theorem (4). In the $\alpha$ method, the effective angle of attack is obtained using sectional lift coefficient computed with Kutta-Joukowski theorem (4) and the known sectional lift curve slope, rather than using the induced angle of attack. Like the Γ method, section lift is interpolated at the effective angle of attack in the database. Section lift and lift curve slope are used to update UVLM sections' angle of attack (UVLM's boundary condition) instead of updating circulation directly. Circulation is recomputed at every iteration by solving UVLM's linear system of equation (3).

The $\alpha$ method is generally preferred as it is unambiguous even in post stall situations, unlike the Γ method, as well as requiring significantly less relaxation to achieve convergence in the non-linear region. The viscous coupling considered in this work is the Van Dam $\alpha$ method [11] as modified by Gallay [1, 12, 13] to remove the dependency of the viscous slope in the coupling algorithm. In this modified $\alpha$ method [1, 2, 4, 5, 12–14], the control points are adapted to reflect a slope of $C_{l\alpha} = 2\pi$ in the UVLM. The algorithm is as follow:

1) Solve the UVLM to obtain the circulation distribution.
2) **for** every spanwise section **do**:
3) Compute $C_{l,inviscid}$ using Kutta-Joukowski theorem (4).
4) Calculate the effective angle of attack (8) knowing the slope of $C_{l\alpha} = 2\pi$:

$$\alpha_e = \frac{C_{l,inviscid}}{2\pi} - \alpha_{local} + \alpha_{3D} \tag{8}$$

with $\alpha_{local}$ the iterated variable initially set to section's free stream angle of attack $\alpha_{3D}$.

5) Interpolate the viscous lift ($C_{l,visc}$) at the effective angle of attack from a database.
6) Update the local angle of attack (9) in the right hand side of the UVLM's linear system of equation (3):

$$\alpha_{local} = \alpha_{local} + \left(\frac{C_{l,inviscid} - C_{l,visc}}{2\pi}\right) \cdot relaxationFactor \tag{9}$$

7) **end for**.
8) Repeat steps 1-7 until convergence.

Convergence of the viscous coupling algorithm means that the lift at each spanwise section in the UVLM is the same as that of the local 2D database associated to that section, while still enforcing a modified UVLM boundary condition. This modification is simply a change in the free stream angle of attack. This coupling procedure is very efficient because it requires no geometry handling, even for important profile geometry deviation from the UVLM thin airfoil, as the effects are included numerically by the procedure via the database. When convergence is obtained, effective angle of attack is known at every station, enabling the interpolation of any other profile coefficient such as 2D drag, moment or heat transfer. Remembering that classical UVLM is a potential (inviscid) method, it can only model induced drag. Viscous coupling adds the possibility to include profile drag at converged lift coefficients. The method is general enough to handle the incorporation of any effect which can be reduced to local $C_{l\alpha}$ and $C_{d\alpha}$ (profile viscosity, compressibility, sweep cross-flow (2.5D), centrifugal-Coriolis forces, ice accretion or control surface deflection) [1–5], given that a 2D database of the effects can be constructed. The computational cost of the viscous coupling is thus mostly encapsulated by the construction of the databases, which needs to be done only once per profile/condition to be tested. The runtime cost of this algorithm is very small compared to the most time consuming parts of the UVLM algorithm.

## V. Methodology

### A. Computational framework

The NL-UVLM algorithm described above has been implemented in an in-house C++ shared memory code parallelized using OpenMP. Validation of this code in fixed wing application has been performed in earlier works [2, 5, 14]. NL-UVLM is compared with higher fidelity URANS 3D results produced with STAR-CCM+ ($k - \omega$ SST turbulence model). All the results were generated on Compute Canada's supercomputer Beluga (40 cores, 2 x Intel Gold 6148 Skylake @ 2.4 Ghz per node). NL-UVLM simulations ran for 2h on 1 node (40 cores) while URANS 3D results took about 1 week on 6 nodes (240 cores).

### B. Test case definition

The geometry chosen represents a simplified version of the S-76 rotor. This choice helped to reduce the simulations complexity while still obtaining meaningful rotary-wing results. The differences between this simplified version

and the actual S-76 rotor are underlined in table 1. The number of blades was reduced from 4 to 2 to reduce the computational cost (especially for the URANS 3D). The profile was kept to a constant uncambered NACA0012 to reduce geometry-induced uncertainties during code verification. Finally, hovering cases were avoided as a small rate of climb helps to convect the vortex away from the rotor and simplifies the far field boundary conditions in the URANS 3D. One disadvantage of this simplified geometry is that comparison with actual experimental data is harder to conduct. As only preliminary results are sought, URANS 3D will be considered as the expected solution, though further validation will be necessary.

| | S-76 | S-76-Mod. |
|---|---|---|
| $N_{blades}$ | 4 | 2 |
| Airfoil | SC10(13-95) | NACA0012 |
| $R_{tip}$ | 1.42 m | 1.42 m |
| $R_{root}$ | 0.2698 m | 0.2698 m |
| $M_{tip}$ | 0.55, 0.6, 0.65 | 0.60 |
| $c$ | 0.0787 m | 0.0787 m |
| Linear twist | -10 deg | -10 deg |
| Collective $\theta_{75}$ | [0-12] deg | 6, **9**, 12 deg |
| Rate of Climb $\frac{v_c}{v_{tip}}$ | 0 | 0.01, **0.02**, 0.03 |

**Table 1 Comparison between actual S-76 and simplified test case considered in this work**

### C. UVLM simulations

Figure 2 shows a sample of solution using NL-UVLM for the test case defined in subsection V.B. On the left of this figure, it can be seen that the wake is free of the singularities and well developed below the rotor plane, extending far enough for the coefficients to have reached steady state. On the right, a zoom on the rotor plane reveals that the tip vortex and close wake contraction are qualitatively well captured. Note that cosine tip mesh refinement is used as rotary aerodynamic forces vary rapidly in that region. Also, all simulations were run for 20 rotations with 20 iterations to reach full rotational speed (to avoid a large starting vortex).

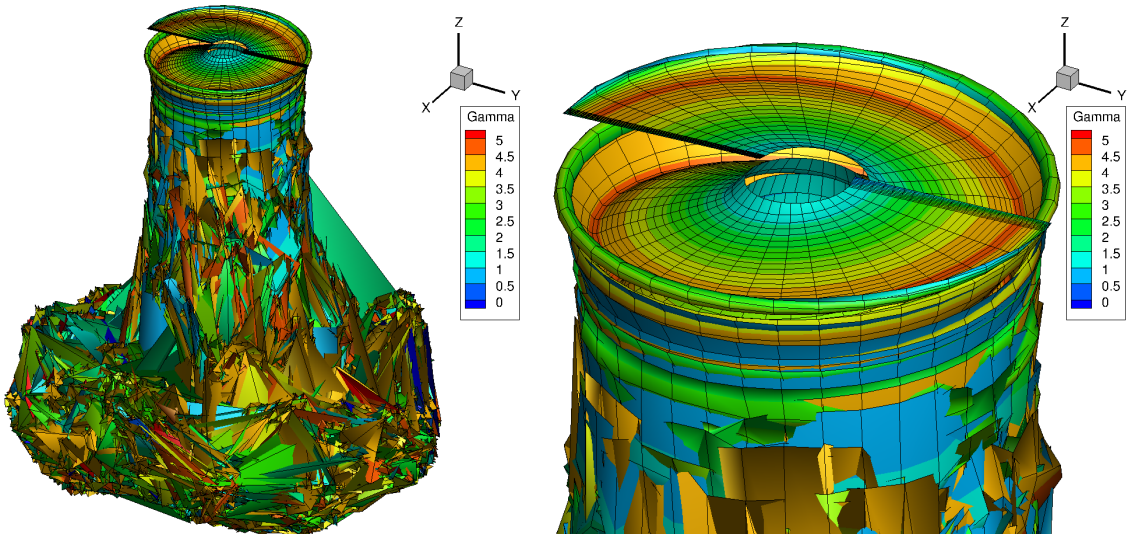


**Fig. 2 Test case wake development a) Rotor and wake b) Zoom on rotor**

### D. Convergence Study

A convergence study was done to investigate the effect of different parameters on the results. Table 2 shows the results of that study, where Panels stands respectively for the number of spanwise and chordwise panels per blade, $\Delta\Psi$ the azimuthal increment between two time step (in degrees), $r_c$ the smoothing parameter as defined in subsection III.E (% of blade chord), $t_{wall}$ time resources required on the supercomputer (in hours), $\Delta C_T$ the difference in the coefficient of thrust with the fine case (in %) and $\Delta$ FM the difference in the Figure of Merit with the fine case (in %).

| Panels | $\Delta\Psi(^\circ)$ | $r_c(\%)$ | $C_T$ | FM | $t_{wall}(h)$ | $\Delta C_T(\%)$ | $\Delta$ FM(%) |
|---|---|---|---|---|---|---|---|
| 30x8 | 5 | 10 | 0.0034054 | 0.70810 | 15 | - | - |
| 30x8 | 10 | 10 | 0.0034036 | 0.70812 | 2 | -0.05 | 0.002 |
| 30x8 | 10 | 0 | 0.0034034 | 0.70812 | 2 | -0.06 | 0.003 |
| 15x4 | 10 | 10 | 0.0034112 | 0.70785 | 0.5 | 0.17 | -0.036 |

**Table 2 Effect of refinement on simulations' results**

The overall coefficients in the table appear to be well converged for all the cases, even without the smoothing radius. This is because the coefficients shown are averaged over the last rotation. In the case of singular Biot-Savart, there are still some oscillations in the coefficients after that time. To avoid random errors caused by the singularity, the smoothing radius $r_c = 10\%$ is chosen in the rest of this work. The medium level refinement of 30x8 panels (per blade) with $\Delta\Psi$ of $10^\circ$ was considered accurate enough for this study, yielding 730 iterations to reach the full 20 rotations per simulation.

### E. Verification of the coupling algorithm

The classical UVLM follows the sectional thin airfoil theory of $C_l = 2\pi\alpha$. To verify the viscous coupling algorithm implementation, viscous sections of different lift and drag were inputed to the method. The left handed side of figure 3 shows these results with the lift coefficient $C_l = k_1 2\pi\alpha$ and the drag $C_d = k_2 2\pi\alpha$, where $k_1 > 1$ corresponds to a sectional lift higher than the UVLM, $k_1 < 1$ indicates less lift, $k_1 = 1$ should result in the UVLM and $k_2 > 0$ indicates viscous drag. We clearly see that sectional lift (and thus overall lift) increases with $k_1$. $C_l = 2\pi\alpha$ results in the UVLM as expected, whether viscous drag is present or not. Drag only affects the overall coefficient of power, but not the coupling algorithm.

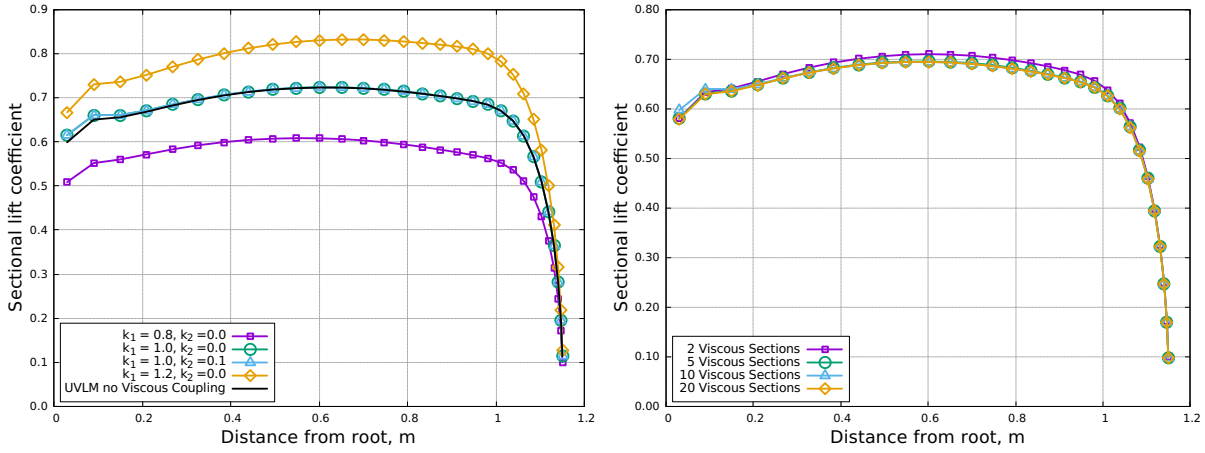


**Fig. 3 Sectional lift coefficient a) Verification with simple cases and b) Convergence with the number of viscous spanwise sections**

### F. Viscous Database

Two hypothesis are made in the generation of the viscous databases. Firstly, only the rotational velocity magnitude is used in the databases, as the added component for the relatively small climb speed is hypothesized negligible on

the total velocity magnitude. Note that this impacts only the Reynolds and Mach numbers, but not the angle of attack as it is calculated by the UVLM. This hypothesis enabled the use of the same databases for all climb speeds considered. Secondly, the effects of centrifugal and Coriolis forces are disregarded. When doing a 2D slice on a blade, the computation is performed in a rotational frame of reference. These effects are not generally negligible, but even without it, a viscous database should perform better than the general thin airfoil theory of the classical UVLM. Further study will be dedicated to that hypothesis in future work.

For fixed wing applications, Van Dam [11] states that at least the root and tip viscous data are required, but that additional stations should be used along the wing if there exists a significant variation in the spanwise airfoil geometry. In the previous section, a single database was used at all the spanwise section. For rotary-wings, even if the chord and profile remain constant, the sectional coefficients can change rather dramatically between the root and the tip, because of the rotational speed. As we move outboard of the wing, the velocity increases, changing the Reynolds and Mach numbers. So even though the geometry is the same, the properties of the flow are expected to change along the span of the wing. It is then expected that 2 viscous stations might not be enough for rotary-wing application. 20 sections along the blade span were computed using in-house RANS 2D [15] (Steady and Sparat-Allmaras turbulence model). Note that using steady databases does not result in a limitation for the considered test case, as the condition is azimuthally independent and enough rotations are simulated to reach full steady state on the blades. Figure 4 shows 10 of these 20 sections. As the Reynolds and Mach numbers change, the angle of attack at which non-linearities begin to appear and the lifting slope in the linear region change. The dashed lines show for reference a purely incompressible thin airfoil $C_l = 2\pi\alpha$ and the Prandtl-Glauert correction applied for the maximum Mach number considered in the test case (Mach = 0.6). Also shown for reference is the maximum effective angle of attack computed in the UVLM for the test case considered. Everything happening on the right handed side of this vertical line can be ignored as it is not used for the present test case. From this figure, it can already be expected that the viscous coupling should be well approximated from UVLM with Prandtl-Glauert correction at lower collective angle, but should differ as the collective increases, especially in the higher Mach numbers (near the tip).

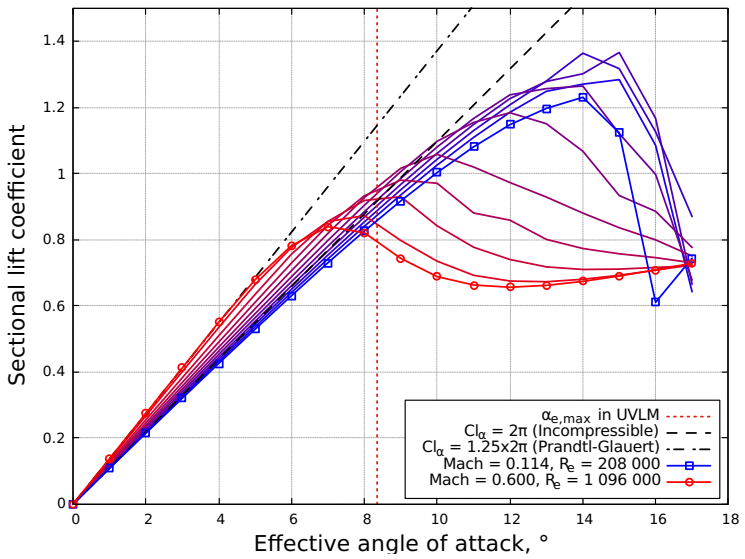


**Fig. 4 NACA0012 lift curves showing 10 of the 20 sections computed**

### G. Convergence with the number of spanwise sections

As stated in the previous section, an investigation of the number of viscous station is required for the rotary-wing application. The right handed side of figure 3 shows the convergence of the sectional lift coefficient as the number of viscous sections increases. It turns out that for this rather simple case, Van Dam's statement still holds in the rotary-application. Some small differences are observable when using only 2 (root an tip) databases, but as the number increases, sectional lift coefficient seems to converge quickly. The added runtime to the UVLM simulations for 20 viscous sections along the span is about 15s (0.2% of the total simulation). Because of the very small increase in time

and the availability of the databases, the other test case were also run using 20 sections.

## VI. Preliminary results

### A. Coefficient of Thrust ($C_T$)

Figure 5 shows the results of the $C_T$ for constant rate of climb (with varying collective angle) and constant collective angle (with varying rate of climb). Further investigation will be required to understand why the classical UVLM overshoots the $C_T$ compared with the URANS 3D. The important takeaway from that figure is the comparison between the UVLM methods, as the viscous coupling is applied on the UVLM and the URANS 3D is a completely different method.

One can see that the viscous coupling falls in between the incompressible UVLM and the UVLM with compressible correction. This is an expected result, as the test case has a Mach number ranging from 0.114 to 0.6, so the lift is expected to be increased in the pre-stalled region compared with the incompressible UVLM, but as the collective angle ranges from 6 to 12 degrees, it is also expected that some of the lifting sections experience non-linearities in the lift slope, reducing the lift compared with the UVLM with Prandtl-Glauert correction. The left handed side figure confirms the prediction made at the end of subsection V.F of this paper, that the difference between the Prandtl-Glauert corrected UVLM and the viscous coupling increases with the collective. Similar behavior is less obviously observed for varying rate of climb.

These results show that the use of the viscous coupling incorporating compressible RANS 2D databases at different spanwise sections implicitly incorporates both compressibility and non-linear effects in the UVLM without having to add specific corrections.

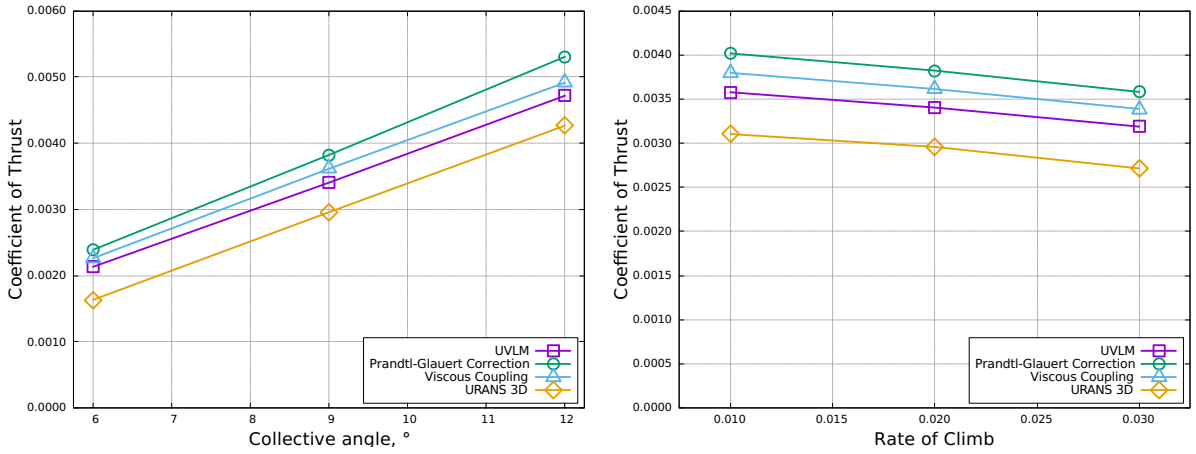


**Fig. 5 Coefficient of Thrust with a) Rate of climb = 0.02 b) Collective angle = 9**

### B. Spanload

Figure 6 shows the detailed spanload which displays a similar trend as the previous figure. It is worth noting that the spanload shape of the UVLM simulations is similar to that of the URANS 3D, but the amplitude is overestimated. The viscous coupling is well represented by both the UVLM incompressible and the Prandtl-Glauert corrected at low Mach number (near the root of the blade). In the higher Mach numbers, for the small collective and high rate of climb, the Prandtl-Glauert corrected UVLM better predicts the viscous coupling because the angle of attack of blade sections remains small, keeping the viscous databases near the linear region. When the local angle of attack is increased, the Prandtl-Glauert correction overestimates the local lift because it does not take non-linearities into account.

### C. Sectional effective angle of attack

Figure 7 shows the distribution of the effective angle of attack along the blade. Only incompressible UVLM and viscous coupling are shown, because effective angle of attack in URANS 3D is not trivial to recover and Prandtl-Glauert

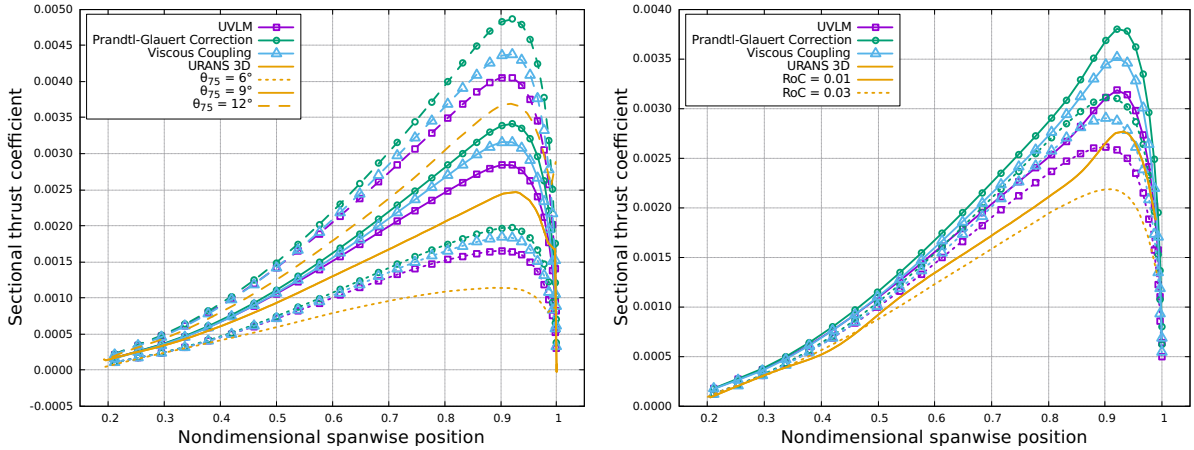


**Fig. 6 Sectional coefficient of thrust with a) Rate of climb = 0.02 b) Collective angle = 9**

corrected would be the same curve as the UVLM. That figure pictures how the algorithm effectively modifies the boundary condition along the blade to be lower in the region where lift is higher in the databases and inversely in order to respect the flow tangency at the collocation points.

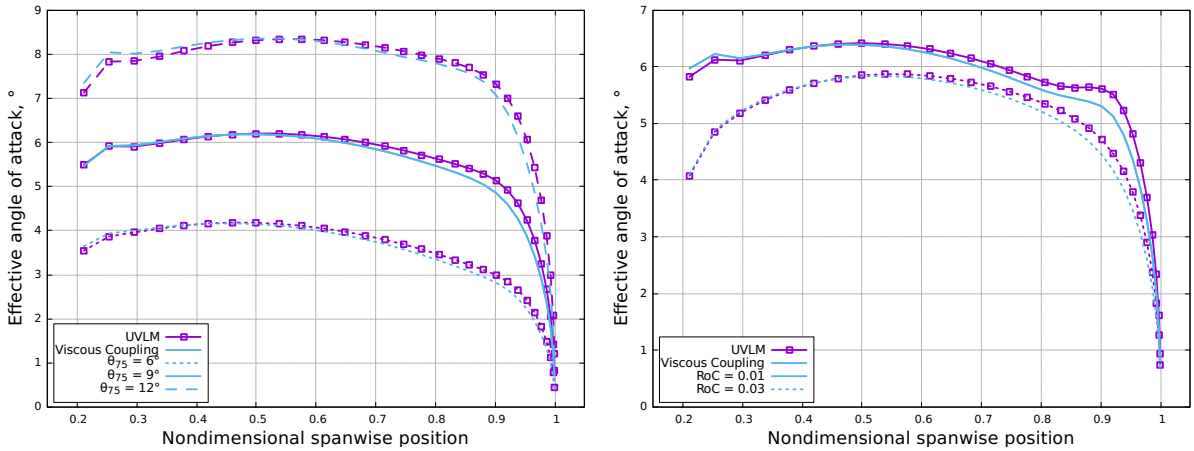


**Fig. 7 Sectional effective angle of attack with a) Rate of climb = 0.02 b) Collective angle = 9**

### D. Figure of Merit (FM)

The drag computed with incompressible and Prandtl-Glauert corrected UVLMs is only the induced drag. Viscous coupling adds sectional profile and viscous drag to this induced drag. It is therefore expected that the FM should be improved by the viscous coupling when compared with the URANS 3D. Figure 8 shows just that. Generally speaking, when staying clear of stalled conditions, at higher $C_T$, FM is mostly driven by the induced power (caused by the induced drag) and at lower thrust, profile and viscous drag become more dominant. That is why inviscid UVLMs seem to better predict the FM, especially with the Prandtl-Glauert correction, as the induced power is high. At lower collective, the viscous effects are not negligible. FM does not vary linearly with $C_T$, so is expected to be different for a given condition (collective and rate of climb) if the computed $C_T$ is different. That might explain the growing difference between the viscous coupling and the URANS 3D as the collective is lowered, since the offset in $C_T$ is proportionally more important than at higher $C_T$.

A fairer comparison is to plot the FM as a function of $C_T$. However, inflow velocity (climb speed) can also have an impact on the actual FM, so to reduce uncertainties, only the simulations at constant climb speed are shown in figure 9. These initial results are very encouraging, showing good agreement for FM vs $C_T$ of viscous coupling with URANS 3D,

although more data would be necessary before drawing general conclusions.

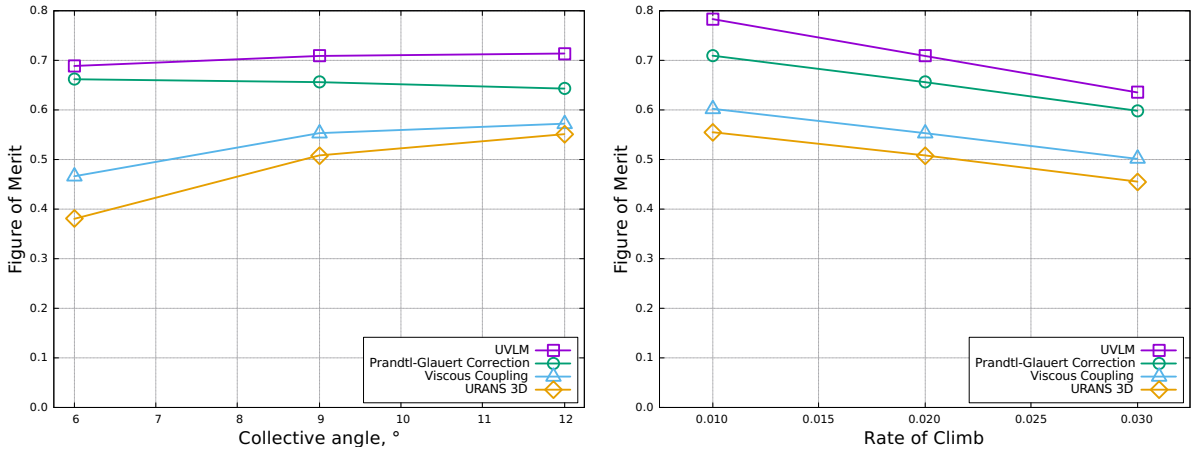


**Fig. 8 Figure of Merit with a) Rate of climb = 0.02 b) Collective angle = 9**

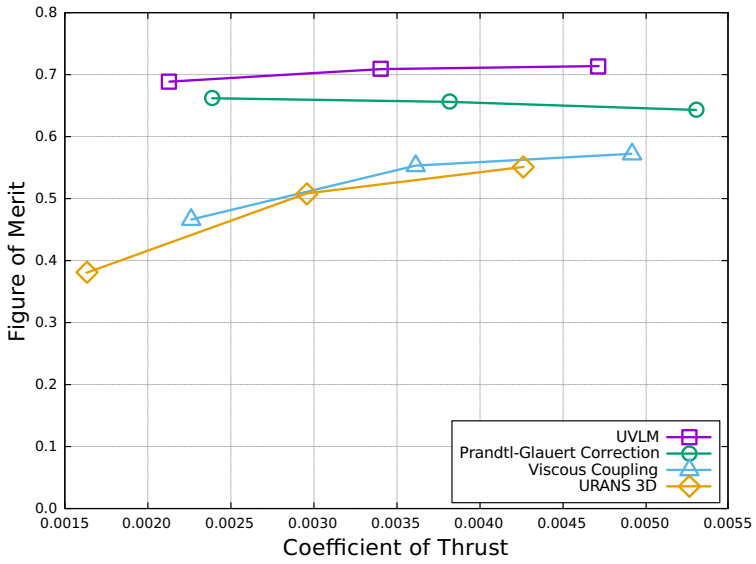


**Fig. 9 Figure of Merit versus coefficient of thrust with Rate of climb = 0.02**

## VII. Conclusion

In conclusion, NL-UVLM for rotary-wing aerodynamics has successfully been implemented and tested in the context of a simplified helicopter rotor analysis. Compared with the classical UVLM, viscous coupling has the anticipated effect on $C_T$ and seems to greatly improve FM, although prudence is required since little data has been examined so far. In this work, it was shown that the viscous coupling implicitly added compressibility effects to the classical method, but as a reminder, viscous coupling can incorporate any effect which can be reduced to local $C_{l\alpha}$ and $C_{d\alpha}$ (Compressibility, icing, sweep cross-flow (2.5D), aileron deflection, centrifugal-Coriolis effects). The computational cost is encapsulated in the construction of the databases, but is almost insignificant compared with the rest of the UVLM algorithm.

**Limitations**

1) The simplified geometry used in this work helped the modeling of the test case, but made comparison with other works more difficult. Because it is not a standard test case, it is harder to identify the source of the disparity in the Thrust Coefficient.

2) This simplified geometry only verified the viscous coupling in the simplest cases. Nothing guarantees that the other usage of the viscous coupling still holds true in a rotary-wing application.
3) The assumptions made in the databases (negligible climb speed velocity on the total free stream magnitude of the section and no centrifugal-Coriolis effects) might not be reasonable at every blade station.

## References


[1] Gallay, S., and Laurendeau, E., "Nonlinear Generalized Lifting-Line Coupling Algorithms for Pre/Poststall Flows," *AIAA Journal*, Vol. 53, No. 7, 2015, pp. 1784–1792. doi:10.2514/1.J053530, URL https://arc.aiaa.org/doi/10.2514/1.J053530.

[2] Parenteau, M., Sermeus, K., and Laurendeau, E., "VLM Coupled with 2.5D RANS Sectional Data for High-Lift Design," *2018 AIAA Aerospace Sciences Meeting*, AIAA SciTech Forum, American Institute of Aeronautics and Astronautics, 2018. doi:10.2514/6.2018-1049, URL https://arc.aiaa.org/doi/10.2514/6.2018-1049.

[3] Nguyen, M. T., and Laurendeau, E., "Rotational Effects on Airfoils using 2.5D Reynolds-averaged Navier-Stokes Solver," , 2019. URL https://www.openconf.org/aero2019/modules/request.php?module=oc_proceedings&action=summary.php&id=78&a=Accept.

[4] Bourgault-Cote, S., Parenteau, M., and Laurendeau, E., "Quasi-3D multi-layer ice accretion model using a Vortex Lattice Method combined with 2.5D RANS solutions," *54rd 3AF International Conference on Applied Aerodynamics*, Paris, France, 2019.

[5] Gagnon, M., and Laurendeau, E., "Non-linear coupled VLM/RANS/FEM analysis of control surface reversa," *53rd 3AF International Conference on Applied Aerodynamics*, Salon-de-Provence, France, 2018.

[6] Katz, J., and Plotkin, A., *Low-Speed Aerodynamics*, Cambridge University Press, 2001. Google-Books-ID: rAS1DmBRLo8C.

[7] Melin, T., Isikveren, A., and Friswell, M., "Induced-Drag Compressibility Correction for Three-Dimensional Vortex-Lattice Methods," *Journal of Aircraft - J AIRCRAFT*, Vol. 47, 2010, pp. 1458–1460. doi:10.2514/1.C000197.

[8] C. A. Ferlisi, and Eric Laurendeau, "Development of a Medium-Fidelity Rotorcraft Aerodynamic Simulation Tool," *CASI AERO Conference 2017*, Toronto, 2017. URL https://www.openconf.org/aero2017/modules/request.php?module=oc_proceedings&action=summary.php&id=46&a=Accept.

[9] Bhagwat, J, M., Leishman, and Gordon, J., "Generalized Viscous Vortex Model for Application to Free-Vortex Wake and Aeroacoustic Calculations," AHS International, 2002. URL https://vtol.org/store/product/generalized-viscous-vortex-model-for-application-to-freevortex-wake-and-aeroacoustic-calculations-1996.cfm.

[10] Chattot, J., "Analysis and Design of Wings and Wing/Winglet Combinations at Low Speeds," *Computational Fluid Dynamics Journal*, Vol. 13, No. 3, 2004, pp. 761–99. doi:10.2514/6.2004-220.

[11] van Dam, C. P., "The aerodynamic design of multi-element high-lift systems for transport airplanes," *Progress in Aerospace Sciences*, Vol. 38, No. 2, 2002, pp. 101–144. doi:10.1016/S0376-0421(02)00002-7, URL http://www.sciencedirect.com/science/article/pii/S0376042102000027.

[12] Gallay, S., Ghasemi, S., and Laurendeau, E., "Sweep effects on non-linear Lifting Line Theory near Stall," *52nd Aerospace Sciences Meeting*, 2014. doi:10.2514/6.2014-1105.

[13] Gallay, S., "Algorithmes de couplage RANS et écoulement potentiel," phd, École Polytechnique de Montréal, Feb. 2016. URL https://publications.polymtl.ca/2061/.

[14] Parenteau, M., Plante, F., Laurendeau, E., and Costes, M., "Unsteady Coupling Algorithm for Lifting-Line Methods," *55th AIAA Aerospace Sciences Meeting*, 2017. doi:10.2514/6.2017-0951, URL https://arc.aiaa.org/doi/abs/10.2514/6.2017-0951.

[15] Pigeon, A., Levesque, A., and Laurendeau, E., "Two-dimensional Navier-Stokes flow solver developments at Ecole Polytechnique de Montreal," *CFD Society of Canada 22nd Annual Conference, CFDSC*, Toronto, Canada, 2014.